Progress In Electromagnetics Research B, Vol. 75, 41–57, 2017

Pattern Synthesis of Circular Antenna Array with Directional Element Employing Deterministic Space Tapering Technique

Mavulluri Ganesh* **and Konidala R. Subhashini**

Abstract—This paper proposes the concept of sparse appended with the space tapering technique for the synthesis of an antenna radiation pattern. The procedure experiments on a Circular Antenna Array (CAA) configuration comprising of directional element $(1 + \cos(\phi))$. The sparse initiates the minimum number of active elements in the CAA, while the space tapering technique gives the complex excitations that yield a beam pattern with constraints such as Side Lobe Level (SLL) and Beam Width (BW) in relation to Dolph-Chebyshev radiation pattern. The phase mode analysis, which is an built-in procedure in the proposed technique explores the circular antenna array configuration characteristics. The simulation results justify the effectiveness of the proposed technique for obtaining the desired radiation pattern synthesis.

1. INTRODUCTION

Antennas play a vital role in communications and radar applications [1–5]. For particular an application, radiation pattern synthesis of an antenna is an important task. The pattern synthesis is a selection of antenna parameters, which generates a radiation beam with specified null positions, Side Lobe Level (SLL) and Beamwidth (BW). The SLL plays a major role in the antenna array design. In fact, antenna system performance is greatly influenced by SLL which in turn reflects on the performance of antenna array.

The number of active antenna elements in an array that contributes for the desired radiation pattern should be minimum opening the avenue of sparse concept as that of signal or image construction [6, 7]. Sparse in the antenna array is defined as activating few antenna elements from a uniformly spaced or a periodic array in order to generate the desired radiation pattern. This sparse characteristic is very useful in certain applications such as mobile devices and satellites, particularly for the situation where the weight and size antenna system is extremely limited. Different approaches of sparsity in the antenna array have been reported in [8–12].

In an antenna system, the geometry of the antenna array configuration decides the direction of the radiation pattern. So in order to facilitate the radiation equally in all directions of the azimuth plane (360°), the circular geometrical arrangement is preferred. This feature of the circular configuration aids the evolution of conformal antenna array, hence Circular Antenna Array (CAA) stands as a backbone for the design of conformal antenna arrays. In [13], the authors give an insight for different beam pattern synthesis for CAA with isotropic elements by reconstructing the current distribution from desired beam pattern.

In this paper, we demonstrate a CAA with the directional element acting as an antenna element and having the element pattern as $(1 + \cos(\phi))$. When the radiating elements are directive, the array performance in terms of beam width and pattern stability is usually improved compared to an array with the isotropic elements [14–16]. The array factor for CAA with directional element pattern differs

Received 16 March 2017, Accepted 28 April 2017, Scheduled 16 May 2017
* Corresponding author: Mavulluri Ganesh (ganesh419ece@gmail.com).
The authors are with the National Institute of Technology, Rourkela, India.

from the CAA with isotropic elements. Here space tapering technique is proposed to obtain sparse in the CAA with directional element, and the proposed technique mimics the trapezoidal rule [18]. Generally, the trapezoidal rule focuses on changes between two sample points over a slope of the integral curve, where the space tapering focuses on the inter element angular positions between the antenna elements. The proposed technique provides the degrees of freedom to the antenna element placed at any location in the antenna array and also provides the flexibility between BW and the number of elements (N). Sparse concept on arrays in relation to the BW and number of elements is reported in [17]. The antenna array subjected to space tapering technique provides the reconstructed pattern equivalent to the desired pattern in terms of the main beam and near-side lobes; however the far-out side lobes are slightly deviated [18].

The radius of CAA decides the physical dimension of the array, hence the radius is an important parameter in pattern synthesis. In [21], the value of a harmonic is used to determine the radius array, and in [13], the radius is determined by evaluating a range of values of radii, with analysing the error in the beamwidth and the maximum side-lobe level resultants with respect to the desired pattern. In this article, a new approach is proposed for obtaining the radius of the CAA by utilizing the phase mode concept. The mathematical equations governing the phase mode concept for CAA with both isotropic and directive elements are clearly described and reported [14, 19–22]. Various deterministic procedures on antenna arrays suggest various synthesis procedures for far-field analysis [23–27]. However, this paper aims to relate the far-field analysis in terms of near-field analysis, to synthesize the radiation pattern.

The present paper is organized as follows. Section 2 describes the mathematical formulations for CAA with the directional element. Section 3 presents the demonstration of the case study. Some concluding remarks are summarized in Section 4.

2. MATHEMATICAL FORMULATION

A far-field expression $M(\phi)$ for CAA with directional element function E_L and the model function magnitude G_n and phase α_n is given as [14]

$$M(\phi) = \sum_{n=1}^{N} G_n E_L(\phi - \phi_n) exp(jkr\cos(\phi - \phi_n) + j\alpha_n) \tag{1}$$

where N is the number of antenna elements, G_n the model function excitation amplitude, α_n the model function excitation phase of nth element, E_L the radiation element function, r the circular array radius, ϕ the azimuthal plane, ϕ_n the nth elements azimuth position, j the imaginary unit, and $k = \frac{2\pi}{\lambda}$ the free-space wave number, where λ is the wavelength.

In Equation (1), phase (ϕ_n) is referenced to the center of the circle. As shown in Figure 1, the antenna elements are spaced ϕ_n along the circle, with each element pointing in the radial direction, therefore, the element function cannot be brought outside summation, since it is a function of the element position. But in the case of isotropic elements, the element pattern radiates uniformly in all the directions, so put $E_L(\phi - \phi_n) = 1$, thus Equation (1) can be written for isotropic elements

$$M(\phi) = \sum_{n=1}^{N} G_n \exp(jkr\cos(\phi - \phi_n) + j\alpha_n) \tag{2}$$

2.1. Reconstruction of Model Function or Continuous Excitation Function

Because reconstruction of the model function a desired radiation pattern is essential, in this paper, the conventional Chebyshev pattern is considered. To obtain CAA with sparseness characteristics, the reconstructed model function $G(\varphi) \in C$, in the interval of $-\pi \leq \varphi \leq \pi$, from a desired chebyshev radiation pattern is given as

$$G(\varphi) = \sum_{m=-\infty}^{\infty} \hat{C}_m \exp(jm\varphi) \tag{3}$$

where $\hat{C}_m$ is the coefficients of the series expansion and represents a near-field phase mode coefficient, i.e., $m = 0$ is the first mode with no phase variation along the circumference, but for other phase modes,

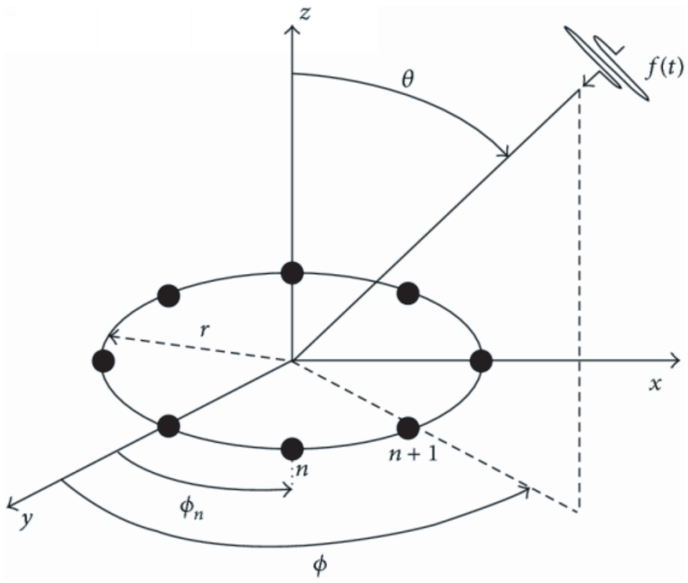

Figure 1. Circular antenna array (CAA).

the phase varies 2π along the circumference of CAA, and due to phase variation, the distortion terms may exist in the model function $G(\varphi)$. $\exp(jm\varphi)$ is orthogonal basis function of order m, and m is the number of phase modes. With $G(\varphi)$ being the continuous excitation model function, the continuous representation of radiated far-field expression for CAA with directional element in the azimuth plane can be written as [14].

$$M(\phi) = \frac{1}{2\pi}\int_{-\pi}^{\pi} G(\varphi)E_L(\phi-\varphi)\exp(jkr\cos(\phi-\varphi))d\varphi \tag{4}$$

where r is the radius of the circular array and ϕ the azimuth plane. The element radiation function E_L is periodic (over 2π), so it can be expanded in a Fourier series given in Equation (5), and its graphical representation is shown in Figure 2.

$$E_L(\varphi) = \sum_{p=-\infty}^{\infty} D_p \exp(jp\varphi) \tag{5}$$

where D_p is element pattern excitation coefficient.

Then, substitute Equation (5) into Equation (4), the obtained far-field pattern expression is given as

$$M(\phi) = \frac{1}{2\pi}\int_{-\pi}^{\pi} G(\varphi)\sum_{p=-\infty}^{\infty} D_p \exp(jp(\phi-\varphi))\exp(-jkr\cos(\phi-\varphi))d\varphi. \tag{6}$$

Now, by expanding the excitation function in terms of phase modes and interchange the integration and summation in Equation (6), the resultant far-field expression can be remodeled as

$$M_m(\phi) = \hat{C}_m \exp(jm\phi)\sum_{p=-\infty}^{\infty}\frac{1}{2\pi}D_p\int_{-\pi}^{\pi}\exp(j(m-p)(\phi-\varphi))\exp(-jkr\cos(\phi-\varphi))d\varphi \tag{7}$$

Therefore, by introducing the Bessel function in Equation (7) the obtained far-field expression is given as [14].

$$M_m(\phi) = [\hat{C}_m\sum_{p=-\infty}^{\infty} D_p j^{m-p}J_{m-p}(kr)]\exp(jm\phi) \tag{8}$$

where $J_{m-p}(kr)$ is the Bessel function of order $(m-p)$ and argument kr. Therefore, the total radiation is the summation of all the phase modes (m). For each phase mode, the sum contributions are from all

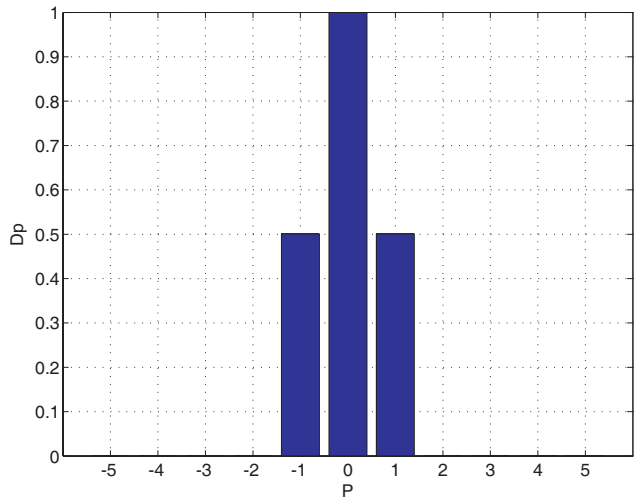

Figure 2. Directional element $(1 + \cos(\phi))$ pattern in Fourier domain.

components D_p of radiating element expansion. On the other hand, the far-field expression for CAA with m phase modes is given as

$$M_m(\phi) = \hat{A}_m \exp(jm\phi) \tag{9}$$

Now by comparing Equations (8) and (9), finally it is possible to calculate the coefficients $\hat{C}_m$ given as

$$\hat{C}_m = \frac{\hat{A}_m}{\sum_{p=-\infty}^{\infty} D_p j^{m-p} J_{m-p}(kr)} \tag{10}$$

Then, Equation (10) will contribute to the reconstruction of the current distribution through $G(\varphi)$.

2.2. Selection of Radius for CAA Design

Providing specified far-field directional radiation pattern in CAA configuration must include the array parameters such as the number of antenna elements (N), array radius (r) and element directional pattern. In pattern synthesis of a CAA configuration, radius is a critical parameter since the near-field excitation coefficients $\hat{C}_m$ are used to calculate the model function $G(\varphi)$. $G(\varphi)$ is too sensitive to small variations of r, and also the near-field excitation coefficients $\hat{C}_m$ are influenced by the Bessel function $J_{m-p}(kr)$. So in this paper, a suitable radius r is determined for synthesis of radiation pattern and the analysis in this paper as follows. First, the desired far-field Chebyshev pattern is considered with constrains such as SLL $= -25$ dB and beam width 107.4°. The mathematical expression for the desired far field in the azimuth plane is given as

$$M(\phi) = \sum_{m=-\infty}^{\infty} \hat{A}_m \exp(jm\phi) \tag{11}$$

where $\hat{A}_m$ is the far-field excitation coefficient for the desired radiation pattern and ϕ the azimuth plane. Now by introducing the phase mode analysis on CAA with directional elements discussed in Section 2.1, the radiation field pattern in terms of the near field excitation coefficients $\hat{C}_m$ is formulated as

$$M(\phi) = \sum_{m=-\infty}^{\infty} \sum_{p=-\infty}^{\infty} [\hat{C}_m D_p j^{m-p} J_{m-p}(kR)] \exp(jm\phi) \tag{12}$$

where $\hat{C}_m$ is the near field excitation coefficient, D_p the element pattern excitation coefficient, and $J_{m-p}(kr)$ the Bessel function with order $(m - p)$ and argument kr.

Now the radius is evaluated by considering the error between the desired radiation pattern near SLL (dB) value (that is −25 dB our case) and near SLL (dB) values obtained from Equation (12) for various r values. For example, for $r = 0.8555\lambda$ the difference between near SLL (dB) value of desired pattern and the computed pattern from Equation (12) is approximately 0 dB. Similarly for $r = 0.88\lambda$, the difference is 0.66 dB, and for $r = 0.82\lambda$ the difference is −0.89 dB. Therefore, in this way the suitable value of radius ($r = 0.8555\lambda$) is determined with the minimum error in terms of near SLL (dB) values. The graphical representation of the described process to evaluate optimum value of radius to an CAA with minimum error in terms of near SLL (dB) value is shown in Figure 3. This approach conceptually equates the far-field excitation coefficients $\hat{A}_m$ to the near-field excitation coefficients $\hat{C}_m$.

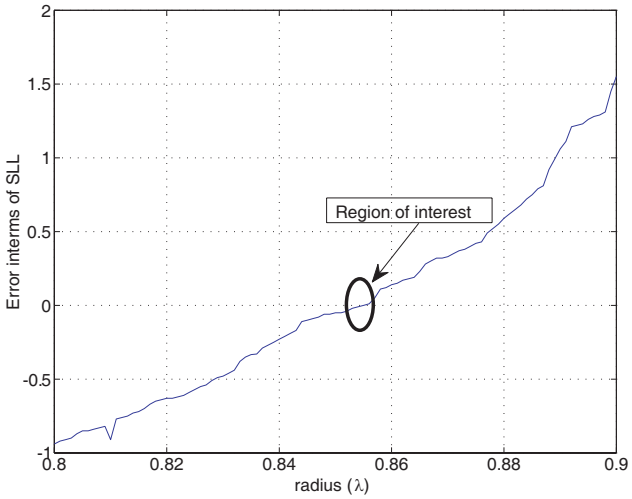

Figure 3. Graphical representation to find a suitable value of radius (R) in terms of minimum difference in near SLL (dB) value.

2.3. Space Tapering over Reconstructed Model Function

In this paper, to obtain the complex excitation for a CAA with sparseness characteristics the proposed space tapering technique procedure is given as below.

Step1: The cumulative current distribution $G_c(\phi)$ of the reconstructed model function of CAA is determined by using Equation (13)

$$G_c(\phi) = \int_{-\pi}^{\phi} |G(\varphi)| r d\varphi \tag{13}$$

where azimuth plane ϕ is the continuous source dimension in the interval of $(-\pi, \pi)$, and r is the radius of the circular array. In this paper, the angular positions of a CAA can be determined by considering only the real part of $G(\varphi)$.

Step 2: The interval $(-\pi, \pi)$ of the continuous source dimension is divided into N sub-intervals of equal lengths, with $N+1$ boundary points $\hat{\phi}_n$. Hence the interval boundaries are defined as $(\hat{\phi}_{n-1}, \hat{\phi}_n)$.

Step 3: The CAA angular positions ϕ_n can be determined in each sub-interval by using Equation (14),

$$G_c(\phi_n) = \frac{G_c(\hat{\phi}_n) - G_c(\hat{\phi}_{n-1})}{2} \tag{14}$$

the projection of $G(\varphi)$ on ϕ determines the antenna element angular position ϕ_n.

Step 4: The complex excitation current in each interval is determined by taking value of $G(\varphi)$ at the position of ϕ_n. Excitation amplitude $|G(\phi_n)|$ and excitation phase $\arg(\phi_n)$ are considered.

3. DEMONSTRATION OF CASE STUDY

The demonstration methodology for case study is shown in Figure 4. For this case study, the desired radiation pattern is considered as the Dolph-Chebyshev pattern with constraints such as SLL = −25 dB, BW = 107.4°. Here the main lobe region is [−53.7° to 53.7°], the near side lobe range [54.5° to 82.6°] and the far side lobe range [82.6° to 180°] in the half of the azimuth plane, and the desired pattern in azimuth plane is shown in Figure 5.

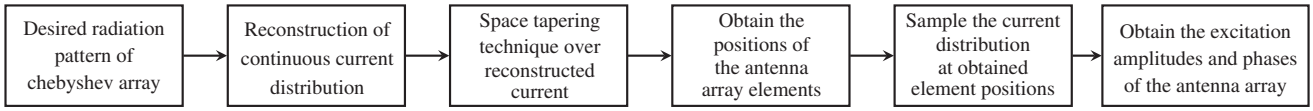

Figure 4. Methodology for the case study.

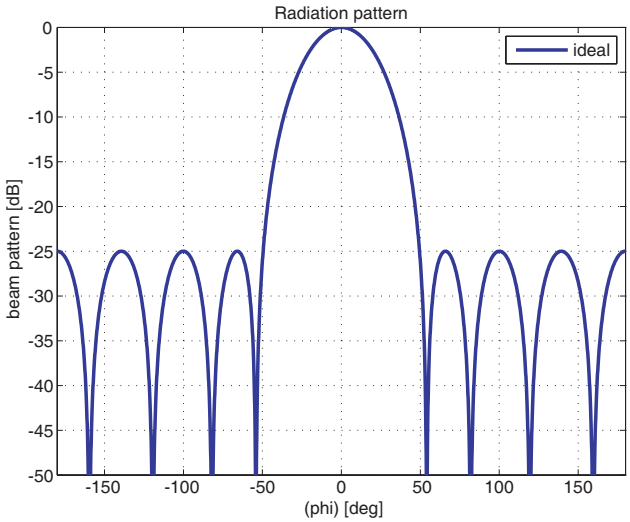

Figure 5. Desired radiation pattern.

Throughout the case study, the number of phase modes is kept constant at $m = 9$, and kr is fixed at 5.37254, based on the criteria discussed in Section 2.2. The fixation of the phase modes at $m = 9$ is validated as follows [14], for obtaining the desired radiation pattern that is Dolph-Chebyshev pattern with constraints such as SLL = −25 dB, BW = 107.4°. In the Linear array with $2N + 1$ elements,the radiation pattern expression is given as [14].

$$M(\phi) = \sum_{n=-N}^{N} V_n \exp(jknd \sin\phi) \tag{15}$$

where V_n is the excitation amplitude of element n, and k is the propagation constant. Similarly for the circular array with $2M + 1$ phase modes, the radiation pattern expression is given as [14].

$$M(\phi) = \sum_{m=-M}^{M} A_m \exp(jm\phi) \tag{16}$$

where A_m is the far-field phase mode coefficient. Therefore, by making each phase mode coefficient A_m equal to corresponding element amplitude V_n identical pattern results from [14, 21]. But in the linear array case, the pattern will be given as a function of $kd \sin\phi$, where as in circular array case, the pattern will be function of the azimuth angle ϕ. And also the basic difference is that in the linear case element excitation V_n directly enters into the pattern function, as CAA case phase mode coefficients or far-field

excitation coefficients A_m instead V_n, and also this phase mode coefficients A_m are influenced by the Bessel function $J_{m-p}(kr)$. So in this paper, based on the above concept, the phase modes $m = 9$ are fixed, for obtaining the the desired radiation pattern that is Dolph-Chebyshev pattern with constraints such as SLL $= -25$ dB, BW $= 107.4°$. The important note is that for obtaining the Dolph-Chebyshev pattern with constraints such as SLL $= -25$ dB, BW $= 107.4°$, we fix the phase modes $m = 9$, but for obtaining different BWs, the phase modes will be changed, for example $m = 7$ and BW $= 141.8°$.

In order to radiate the useful unambiguous mode spectrum in CAA with the directional element, the commonly stated limit to choose the antenna array size by including the phase modes m and argument kr is given as [14].

$$m \leq 2kr + 1 \leq N \tag{17}$$

where m is the number of phase modes and N the number of elements. In our experiment, the number of phase modes is 9 and argument $kr = 5.37254$. So according to Equation (7), the number of elements is initially set as $N = 12$. But according to the relation formulated between phase modes and number

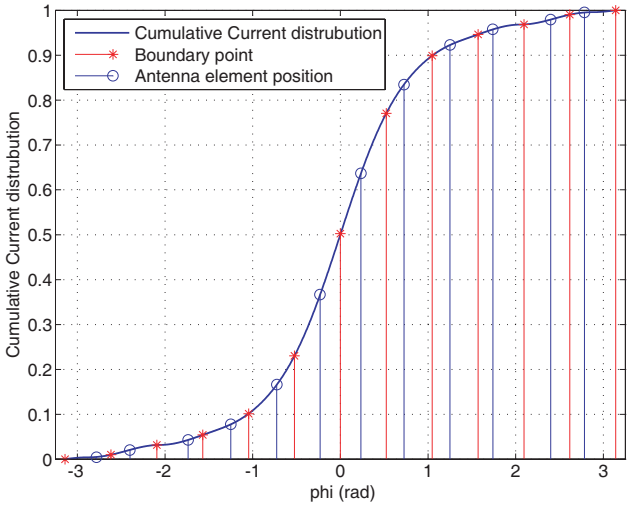

Figure 6. Representation of the Space tapering technique over the cumulative current distribution for $N = 12$.

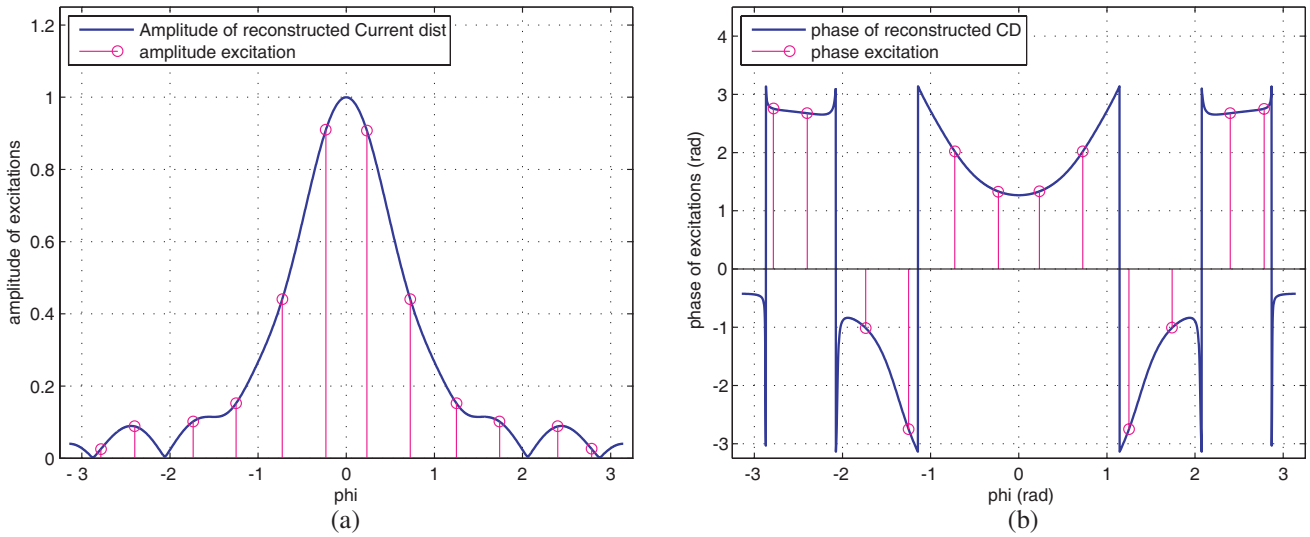

Figure 7. Representation of amplitudes and phases at angular positions for $N = 12$. (a) Amplitude. (b) Phase.

of elements in [21], the minimum requirement of the number of elements N is twice the number of phase modes m, i.e., $N = 2m$ for obtaining an accurate pattern synthesis. So in our case study, the number of elements to experiment with the space tapering technique is $N = 12, 13, 14, 15, 16, 17$ and 18, in order to complete the overall analysis or observe the effect of phase modes and argument kr value on the radiation pattern synthesis. A comprehensive analysis of the proposed procedure for $N = 12$ elements is shown in Figure 6. The corresponding amplitude and phases are shown in Figure 7, and their respective numerical values are tabulated in Table 1.

Table 1. Excitation coefficients obtained for $N = 12$ antenna elements.

n	ϕ_n (rad)	$\lvert G(\phi_n)\rvert$	Arg (ϕ_n) (rad)
1	-2.784	0.02558	2.753
2	-2.4	0.08835	2.676
3	-1.737	0.1019	-1.013
4	-1.25	0.1524	-2.751
5	-0.7261	0.4409	2.018
6	-0.2304	0.9101	1.331
7	0.2339	0.9075	1.333
8	0.7261	0.4409	2.018
9	1.25	0.1524	-2.751
10	1.74	0.1014	-1.008
11	2.4	0.08835	2.676
12	2.78	0.02659	2.752

The corresponding radiation pattern for $N = 12$ is shown in Figure 8.

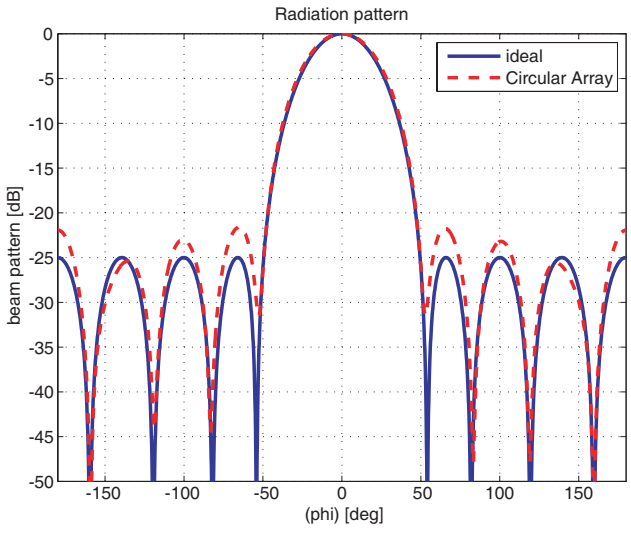

Figure 8. Pattern synthesis with $N = 12$ antenna elements.

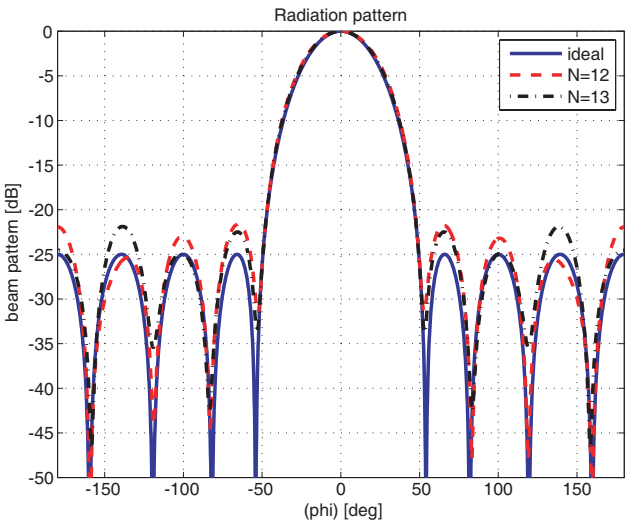

Figure 9. Radiation plot for *ideal*, $N = 12$, $N = 13$.

From Figure 8, the achieved pattern for $N = 12$ elements has a SLL of -21.75 dB and BW $= 107°$, which varies from the design goal by a value of -3.25 dB in terms of near SLL value and $0.4°$ in terms of BW. This deviation is possibly due to spurious effects, i.e., additional distortion terms (harmonics) are not suppressed effectively for $N = 12$ and $m = 9$. So the experiment is continued with the increment in the number of elements (array size) such as $N = 13, 14$ and $N = 15$. The synthesized radiation patterns

by the proposed method are shown in Figures 9, 10, and 11, respectively, and their respective numerical values are tabulated in Table 2 and Table 3, respectively. From Figure 9, the achieved pattern of $N = 13$ elements has an near SLL of -22.5 dB and BW $= 107°$, which varies from the design goal by a value of -2.5 dB in terms of difference in near SLL value and $0.4°$ in terms of difference in BW value. Similarly from Figure 10, the achieved pattern for $N = 14$ elements has an SLL of -22.95 dB and BW $= 107°$, here the SLL and BW vary from the design goal by a value of -2.05 dB in terms of difference in near SLL value and $0.4°$ in terms of difference in BW value, respectively. Here, for $N = 14$ elements, some of the additional distortion terms (harmonics) are suppressed to obtain the close desired pattern compared to the $N = 13$ elements. Therefore, the important observations deduced from Figure 9 and Figure 10, respectively, are that if the array size is increased (i.e, N=13, 14), the value of near SLL matches the desired near SLL value.

So the experiment is continued with the increment in array size for obtaining the desired radiation

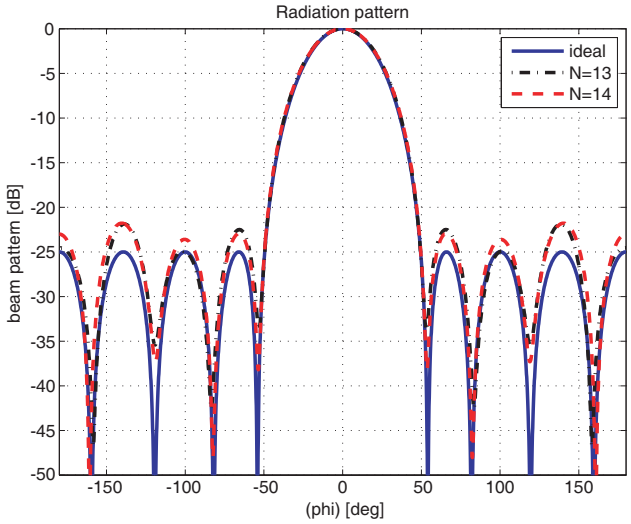

Figure 10. Radiation plot for *ideal*, $N = 13$, $N = 14$.

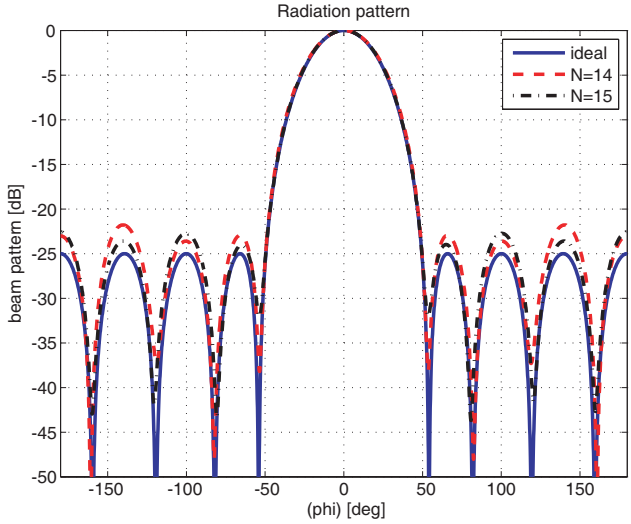

Figure 11. Radiation plot for *ideal*, $N = 14$, $N = 15$.

Table 2. Excitation coefficients obtained for $N = 13$ antenna elements.

n	ϕ_n (rad)	$\lvert G(\phi_n)\rvert$	Arg (ϕ_n) (rad)
1	-2.911	0.009382	-0.4991
2	-2.428	0.08939	2.681
3	-1.824	0.0828	-0.905
4	-1.428	0.1163	-1.924
5	-0.9111	0.3158	2.475
6	-0.4416	0.714	1.518
7	0	1	1.268
8	0.4416	0.714	1.518
9	0.9111	0.3158	2.475
10	1.428	0.1163	-1.924
11	1.824	0.0828	-0.905
12	2.428	0.08939	2.681
13	2.911	0.009382	-0.4991

Table 3. Excitation coefficients obtained for $N = 14$ antenna elements.

n	ϕ_n (rad)	$\lvert G(\phi_n)\rvert$	Arg (ϕ_n) (rad)
1	-2.972	0.02287	-0.4442
2	-2.457	0.08929	2.686
3	-1.925	0.05094	-0.8394
4	-1.56	0.1149	-1.405
5	-1.068	0.232	2.907
6	-0.6301	0.5238	1.816
7	-0.2059	0.9274	1.318
8	0.2059	0.9274	1.318
9	0.6301	0.5238	1.816
10	1.068	0.232	2.907
11	1.56	0.1149	-1.405
12	1.925	0.05094	-0.8394
13	2.457	0.08929	2.686
14	2.972	0.02287	-0.4442

pattern. Now the array size is increased $N = 15$ instead of $N = 14$, and its radiation plot is shown in Figure 11. From Figure 11, we notice that the variation in SLL value and BW is -1.02 dB and 0.1°, respectively with a design goal. Therefore, the observations, deduced from Figures 9, 10, and 11, are such that the near SLL value and BW obtained for $N = 15$ elements and $m = 9$ phase modes are very close to the desired radiation pattern. So a comprehensive analysis of the proposed procedure for $N = 15$ elements and $m = 9$ phase modes is represented in Figure 12. The current excitation magnitudes and phases are shown in Figure 13, and their respective statistical values are given in Table 4. The radiation pattern for $N = 15$ elements and $m = 9$ phase modes is shown in Figure 14. Also from Figure 14, we notice that the obtained pattern is more on the safe side towards the desired radiation pattern of CAA configuration with the directional element $(1 + \cos(\phi))$. But for complete analysis or synthesis of radiation pattern, the experiment is continued with the increment in the array size such as $N = 16, 17$ and $N = 18$. The synthesized radiation patterns by the space tapering technique are shown

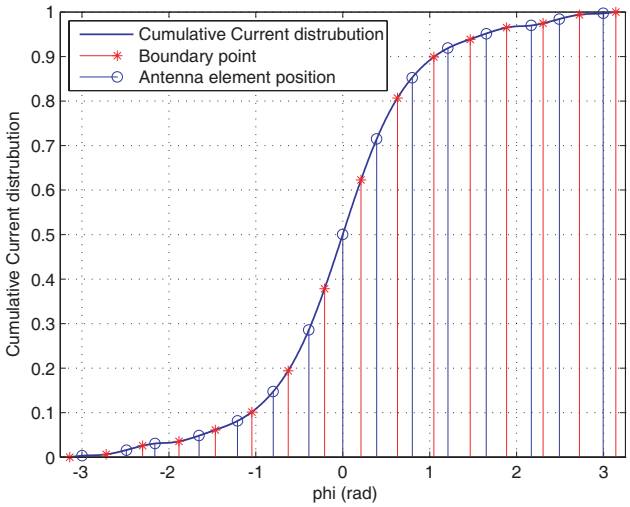

Figure 12. Representation of the Space tapering technique over the cumulative current distribution at $N = 15$.

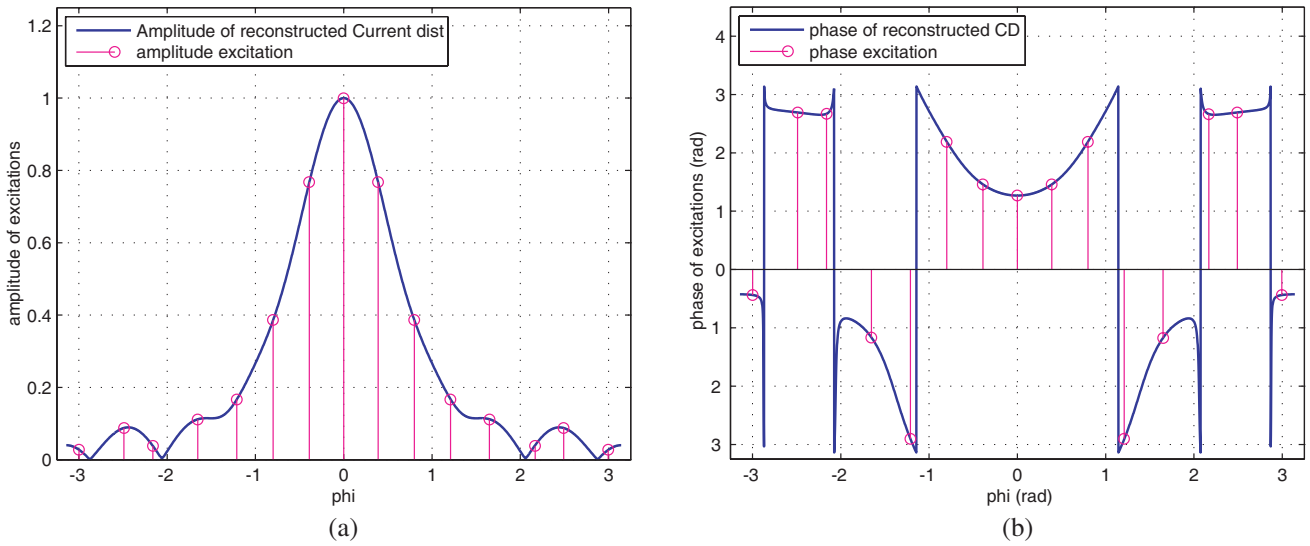

Figure 13. Representation of amplitudes and phases at angular positions for $N = 15$. (a) Amplitude. (b) Phase.

Table 4. Excitation coefficients obtained for $N = 15$ antenna elements.

n	ϕ_n (rad)	$\lvert G(\phi_n)\rvert$	Arg (ϕ_n) (rad)
1	-2.998	0.02765	-0.437
2	-2.489	0.08787	2.692
3	-2.161	0.03781	2.67
4	-1.653	0.1119	-1.165
5	-1.211	0.1668	-2.903
6	-0.7994	0.3863	2.191
7	-0.3892	0.7678	1.458
8	0	1	1.268
9	0.3892	0.7678	1.458
10	0.7994	0.3863	2.191
11	1.21	0.1668	-2.903
12	1.649	0.1119	-1.172
13	2.169	0.03781	2.665
14	2.491	0.08787	2.692
15	2.995	0.02765	-0.4378

in Figures 15, 16 and 17, and numerical excitation values are given in Table 5 and Table 6. As shown in Figure 15, the achieved pattern for $N = 16$ elements has a near SLL of -23.54 dB and BW $= 107.3°$, but the near SLL value varies from design goal by a value of -1.46 dB in terms of difference in SLL value and $0.1°$ in terms of difference in BW value. Similarly from Figure 16, for $N = 17$ elements the near SLL value and BW deviate from the desired radiation pattern by values of -1.83 dB and $0.1°$, respectively. Finally, the experiment is performed on $N = 18$ elements, and the achieved pattern has an SLL of -22.78 dB and BW $= 107.4°$, which varies from the design goal by a value of -2.22 dB in terms of difference in SLL value and $0°$ in terms of difference in BW value. The observation deduced from Figure 17 is that BW exactly matches the desired radiation pattern. Also the observations deduced from the Figures 15, 16, and 17 are the tradeoff between the near SLL value and BW, i.e., if near SLL value increases, but BW is perfectly matching to the desired radiation pattern.

Table 5. Excitation coefficients obtained for $N = 16$ antenna elements.

n	ϕ_n (rad)	$\lvert G(\phi_n)\rvert$	Arg (ϕ_n) (rad)
1	−3.016	0.03044	−0.4337
2	−2.52	0.08495	2.698
3	−2.244	0.06307	2.653
4	−1.728	0.1034	−1.027
5	−1.349	0.1255	−2.3
6	−0.9442	0.297	2.562
7	−0.5568	0.595	1.684
8	−0.1833	0.942	1.308
9	0.1833	0.942	1.308
10	0.5568	0.595	1.684
11	0.9442	0.297	2.562
12	1.349	0.1255	−2.3
13	1.728	0.1034	−1.027
14	2.244	0.06307	2.653
15	2.52	0.08495	2.698
16	3.016	0.03044	−0.4337

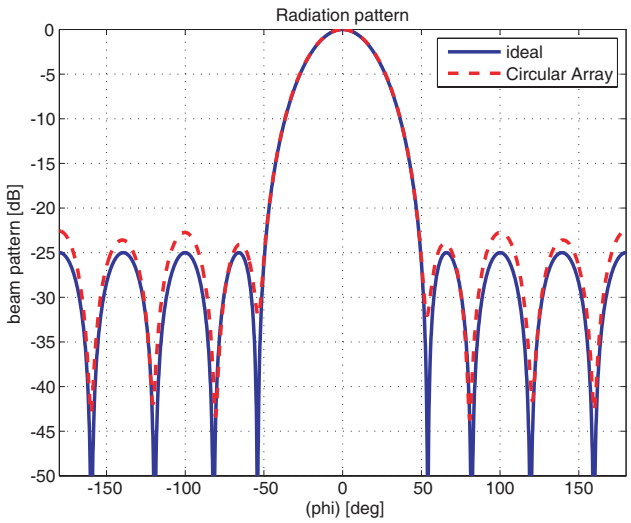

Figure 14. Pattern synthesis with $N = 15$ antenna elements.

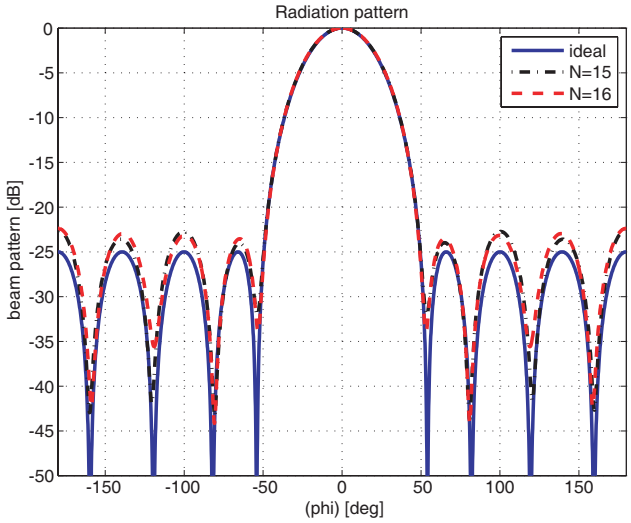

Figure 15. Radiation plot for *ideal*, $N = 15$, $N = 16$.

As shown in Figure 17, for $N = 18$ elements the achieved pattern is very close to the ideal radiation pattern in terms of BW. Therefore, a comprehensive analysis of the proposed procedure for the combination, i.e., $N = 18$, $m = 9$ and $r = 0.8555\lambda$, is represented in Figure 18, and its discrete excitation amplitudes and phases are shown in Figure 19, respectively. Numerical values are tabulated in Table 7. The radiation plot for $N = 18$ antenna elements is shown in Figure 20. From Figure 20, the achieved pattern has an SLL of -22.78 dB and BW $= 107.4°$. Therefore, the space tapering technique validates the statement given in [21], i.e., for obtaining an accurate narrow beam pattern synthesis, the minimum requirement of the number of elements N is twice the number of phase modes m.

In this paper, by applying the space tapering technique comparative numerical values in terms of near SLL and BW obtained for different array sizes along with the remarks are tabulated in Table 8.

Table 6. Excitation coefficients obtained for $N = 17$ antenna elements.

n	ϕ_n (rad)	$\lvert G(\phi_n)\rvert$	Arg (ϕ_n) (rad)
1	−3.026	0.03196	−0.4321
2	−2.548	0.08167	2.703
3	−2.288	0.07333	2.657
4	−1.789	0.09151	−0.943
5	−1.471	0.1148	-1.731
6	−1.072	0.2302	2.917
7	−0.7086	0.455	1.979
8	−0.3491	0.8075	1.419
9	0	1	1.268
10	0.3491	0.8075	1.419
11	0.7086	0.455	1.979
12	1.072	0.2302	2.917
13	1.471	0.1148	−1.731
14	1.789	0.09151	−0.943
15	2.288	0.07333	2.657
16	2.548	0.08167	2.703
17	3.026	0.03196	−0.4321

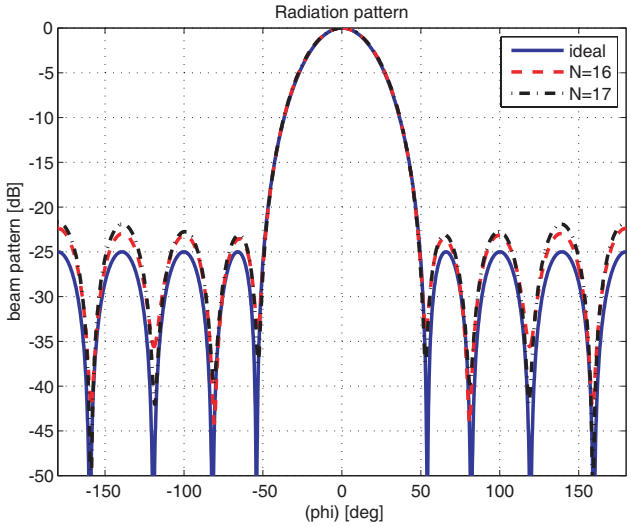

Figure 16. Radiation plot for *ideal*, $N = 16$, $N = 17$.

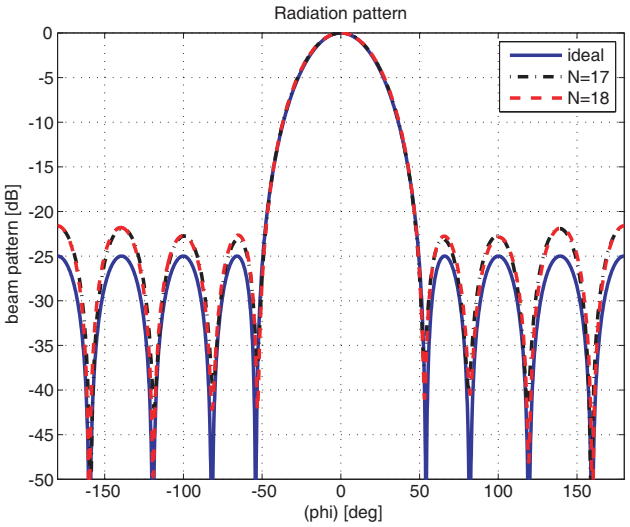

Figure 17. Radiation plot for *ideal*, $N = 17$, $N = 18$.

From the comparison table, it is clearly seen that the desired radiation pattern is closely achieved by $N = 15$ with a minimum error in terms of near SLL and BW instead of $N = 18$ elements. In the case of $N = 18$ elements, the near SLL deviates by a design goal of -2.12 dB where as in $N = 15$ elements the near SLL deviates by a design goal of -1.02 dB. So the space tapering technique gives the tradeoff in objective array sizes in CAA with the directional element. The concept of sparse is clearly observed by synthesizing the radiation pattern with the space tapering technique for $N = 18$ elements and $N = 15$ elements. The $N = 15$ elements for chosen radius ($r = 0.8555\,\lambda$) gives almost desired pattern in terms of both SLL and BW.

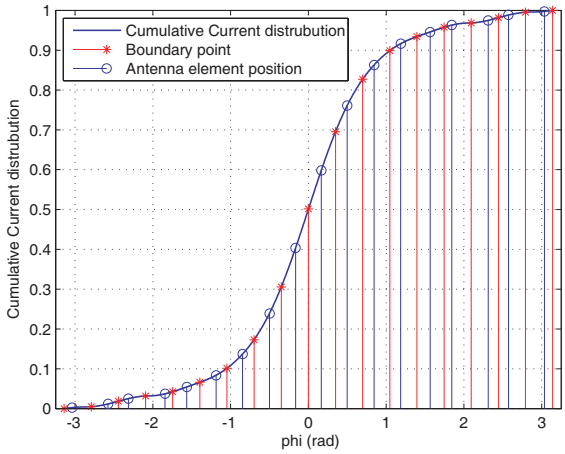

Figure 18. Representation of the Space tapering technique over the cumulative current distribution at $N = 18$.

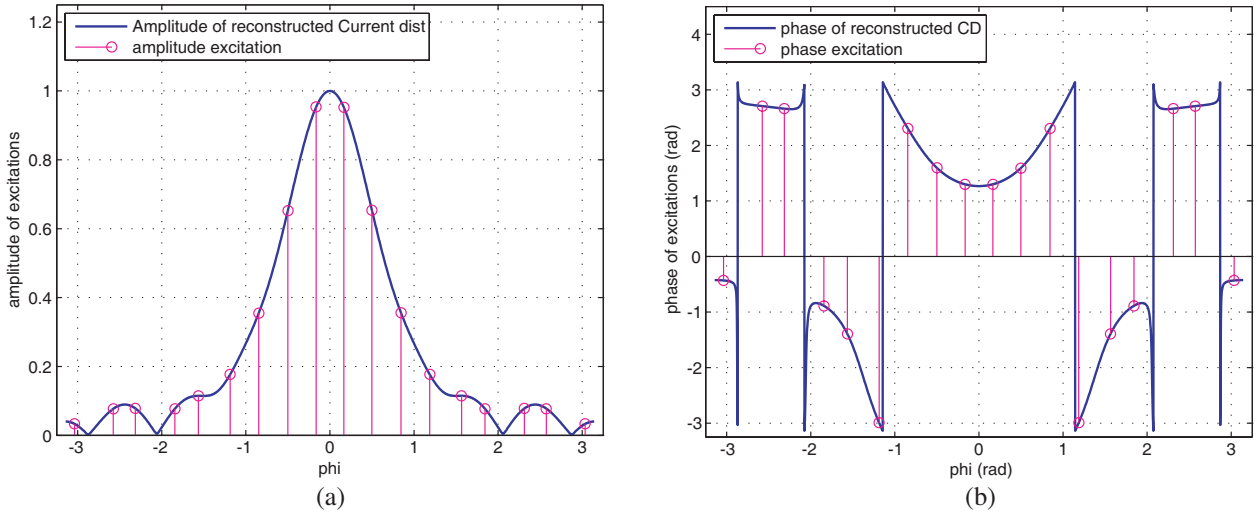

Figure 19. Representation of amplitudes and phases at angular positions for $N = 18$. (a) Amplitude. (b) Phase.

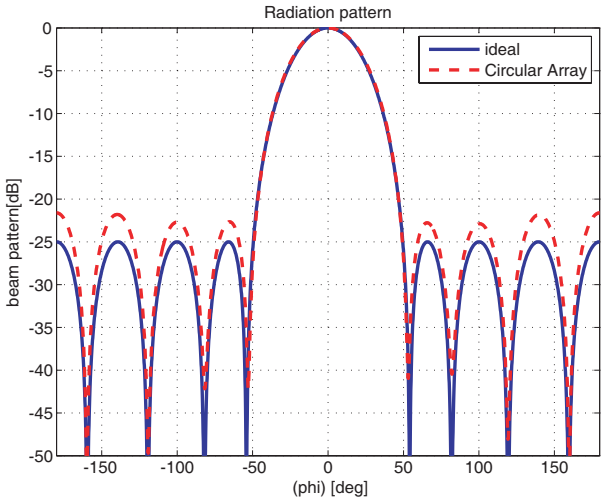

Figure 20. Pattern synthesis with $N = 18$ antenna elements.

Table 7. Excitation coefficients obtained for $N = 18$ antenna elements.

n	ϕ_n (rad)	$\lvert G(\phi_n)\rvert$	Arg (ϕ_n) (rad)
1	−3.037	0.03336	−0.4307
2	−2.576	0.0773	2.707
3	−2.314	0.07836	2.661
4	−1.843	0.07746	−0.8871
5	−1.564	0.1149	−1.394
6	−1.187	0.1768	−2.993
7	−0.8465	0.355	2.308
8	−0.5009	0.6522	1.597
9	−0.1641	0.9532	1.299
10	0.1658	0.9522	1.3
11	0.4992	0.654	1.595
12	0.8447	0.3561	2.304
13	1.187	0.1768	−2.993
14	1.566	0.1149	−1.396
15	1.843	0.07746	−0.8871
16	2.313	0.07836	2.661
17	2.574	0.0773	2.707
18	3.035	0.03336	−04307

Table 8. Comparison table for different antenna array sizes.

No. of elements	Ideal		Space tapering method		Remarks
	BW (deg)	SLL (dB)	BW (deg)	SLL (dB)	
12	107.4	−25	107	−21.75	Not perfectly matched to ideal, deviated by a design goal of near SLL = −3.25 dB and BW = 0.4°
13	107.4	−25	107	−22.5	Not perfectly matched to ideal, deviated by a design goal of near SLL = −2.5 dB and BW = 0.4°
14	107.4	−25	107	−22.95	Not perfectly matched to ideal, deviated by a design goal of near SLL = −2.05 dB and BW = 0.4°
15	107.4	−25	**107.3**	**−23.98**	**Very closed to ideal radiation pattern**
16	107.4	−25	107.3	−23.54	Not perfectly matched to ideal, deviated by a design goal of near SLL = −1.46 dB and BW = 0.1°
17	107.4	−25	107.3	−23.13	Not perfectly matched to ideal, deviated by a design goal of near SLL = −1.87 dB and BW = 0.1°
18	107.4	−25	**107.4**	−22.78	**Perfectly matched in terms of BW but error in SLL by amount of -2.12 dB**

4. CONCLUSION

This paper demonstrates the space tapering technique for a low side lobe and narrow main beam synthesis of CAA configuration with the directional element $(1 + \cos(\phi))$. The radius which is an important parameter of a CAA configuration is modelled in this paper. A good methodology is evolved to determine the radius of a CAA using the phase mode analysis. The angular placement of the antenna element is found by the proposed technique which in turn helps to find the complex excitations to be provided for each individual element in the array. The case study shows that the proposed technique generates the desired pattern (Dolph-Chebysheve) with a minimum error in terms of SLL and beamwidth using $N = 15$ elements instead of $N = 18$ elements as mentioned in [21] with a sparse of 3 elements. The method also highlights the proper choice of array size plays an important role in the desired pattern synthesis. An extensive numerical analysis has been performed with various array sizes, and their effect on the constraints which are SLL and BW is studied. Throughout the study, the proposed technique is investigated on a CAA made up of directional element, i.e., $(1+\cos(\phi))$ to study the practical importance instead of an isotropic element. As a future scope, this approach can be extended for different desired radiation patterns with multiple objectives. The simulation is performed on an i5 processor with 4 GB RAM and MATLAB R2013a.

REFERENCES

1. Morabito, A. F., T. Isernia, M. G. Labate, M. Durso, and O. M. Bucci, "Direct radiating arrays for satellite communications via aperiodic tilings," *Progress In Electromagnetics Research*, Vol. 96, 107–124, 2009.
2. Toso, G., C. Mangenot, and A. G. Roederer, "Sparse and thinned arrays for multiple beam satellite applications," *The Second European Conference on Antennas and Propagation, 2007, EuCAP 2007*, 11–4, IET, 2007.
3. Jacomb-Hood, A. and E. Lier, "Multibeam active phased arrays for communications satellites," *IEEE Microwave Magazine*, Vol. 1, No. 4, 40–47, IEEE, 2000.
4. Bucci, O. M., T. Isernia, S. Perna, and P. Daniele, "Isophoric sparse arrays ensuring global coverage in satellite communications," *IEEE Transactions on Antennas and Propagation*, Vol. 62, No. 4, 1607–1618, 2014.
5. Caille, G., Y. Cailloce, C. Guiraud, D. Auroux, T. Touya, and M. Masmousdi, "Large multibeam array antennas with reduced number of active chains," *European Conference on Antennas & Propagation*, 1–9, 2007.
6. Wright, J., Y. Ma, J. Mairal, G. Sapiro, T. S. Huang, and S. Yan, "Sparse representation for computer vision and pattern recognition," *IEEE*, Vol. 98, No. 6, 1031–1044, IEEE, 2010.
7. Bruckstein, A. M., D. L. Donoho, and M. Elad, "From sparse solutions of systems of equations to sparse modeling of signals and images," *PSIAM Review*, Vol. 51, No. 1, 34–81, SIAM, 2009.
8. Lager, I. E., C. I. Coman, and L. P. Ligthart, "The shared aperture, sparse array antenna approach to designing broadband array antennas," *The Fifth International Kharkov Symposium on Physics and Engineering of Microwaves, Millimeter, and Submillimeter Waves, 2004, MSMW 04*, Vol. 1, 91–96, IEEE, 2004.
9. Milligan, T. A., "Space-tapered circular (ring) array," *IEEE Antennas and Propagation Magazine*, Vol. 46, No. 3, 70–73, IEEE, 2004.
10. Bucci, O. M. and S. Perna, "A deterministic two dimensional density taper approach for fast design of uniform amplitude pencil beams arrays," *IEEE Transactions on Antennas & Propagation*, Vol. 59, No. 8, 2852–2861, 2011.
11. Bucci, O. M., S. Perna, and D. Pinchera, "Advances in the deterministic synthesis of uniform amplitude pencil beam concentric ring arrays," *IEEE Transactions on Antennas and Propagation*, Vol. 60, No. 7, 3504–3509, IEEE, 2012.
12. Bucci, O. M., T. Isernia, A. F. Morabito, S. Perna, and D. Pinchera, "Isophoric sparse arrays: A synthesis procedure for circularly symmetric shaped beams," *2012 6th European Conference on Antennas and Propagation (EUCAP)*, 832–836, IEEE, 2012.

13. Garza, L. A., L. F. Yepes, D. H. Covarrubias, M. A. Alonso, and M. A. Panduro, "Synthesis of sparse circular antenna arrays applying a tapering technique over reconstructed continuous current distribution," *IET Microwaves, Antennas & Propagation*, Vol. 10, No. 3, 347–352, 2016.
14. Josefssona, L. and P. Perssonb, *Conformal Array Antennas*, Springer, 2015.
15. Longstaff, I. D., P. E. K. Chow, and D. E. N. Davies, "Directional properties of circular arrays," *Proceedings of the Institution of Electrical Engineers*, Vol. 114, No. 6, 713–718, 1967.
16. Rahim, T. and D. E. N. Davies, "Effect of directional elements on the directional response of circular antenna arrays," *IEE Proceedings H — Microwaves, Optics and Antennas*, Vol. 129, No. 1, 18–22, 1982.
17. Bucci, O. M., M. D'Urso, T. Isernia, P. Angeletti, and G. Toso, "Deterministic synthesis of uniform amplitude sparse arrays via new density taper techniques," *IEEE Transactions on Antennas and Propagation*, Vol. 58, No. 6, 1949–1958, 2010.
18. Fang, D.-G., *Antenna Theory and Microstrip Antennas*, CRC Press, 2009.
19. Aumann, H. M., "Phase mode analysis of directional elements in a circular array," *IEEE Antennas and Propagation Society International Symposium, 2008, AP-S 2008*, 1–4, 2008.
20. Suarez, C., M. Ferrando-Bataller, and A. Valero-Nogueira, "Pattern synthesis of uniform circular arrays with directive elements," *IEEE Antennas and Propagation Society International Symposium, 2004*, Vol. 3, 2812–2815, 2004.
21. Davies, D. E. N., "A transformation between the phasing techniques required for linear and circular aerial arrays," *Proceedings of the Institution of Electrical Engineers*, Vol. 112, No. 11, 2041–2045, 1965.
22. Singh, H., K. Lekshmi, D. Poovannan, and R. M. Jha, "Pattern synthesis studies for planar and non-planar conformal arrays," National Aerospace Laboratories, 2007.
23. Al-Husseini, M., E. Yaacoub, K. Y. Kabalan, and A. El-Hajj, "Pattern synthesis with uniform circular arrays for the reduction of WCDMA intercell interference," *Turkish Journal of Electrical Engineering & Computer Sciences*, Vol. 16, No. 3, 207–215, 2008.
24. Jones, M. R. and H. D. Griffiths, "Broadband pattern synthesis from a circular array," *Sixth International Conference on Antennas and Propagation, 1989, ICAP 89*, Conf. Publ. No. 301, 55–59, 1989.
25. Xu, Z., H. Li, Q.-Z. Liu, and J.-Y. Li, "Pattern synthesis of conformal antenna array by the hybrid genetic algorithm," *Progress In Electromagnetics Research*, Vol. 79, 75–90, 2008.
26. Wang, T.-E., R. Brinkman, and K. R. Baker, "Dolph-Chebyshev pattern synthesis for uniform circular arrays," *Wireless at VT*, 1–9, 2011.
27. De Abreu, G. T. F. and R. Kohno, "A modified Dolph-Chebyshev approach for the synthesis of low sidelobe beampatterns with adjustable beamwidth," *IEEE Transactions on Antennas and Propagation*, Vol. 51, No. 10 3014–3017, 2003.